Study on the Breakdown Characteristics of Multiple-Reignition Secondary Arcs on EHV/UHV Transmission Lines

Runchang Li, Hongshun Liu, *Member, IEEE*, Xiaoxuan Lou, Ping Song, Weihong Hou, Shiqiang Dai, Yuchao Shi, Gongyu Jin, Wah Hoon Siew, *Senior Member, IEEE*, and Qingmin Li, *Member, IEEE*

***Abstract*—A long-gap AC arc with a length of more than ten meters (secondary arc) are normally generated at the short-circuit arc channel after a single-phase-to-ground fault. In previous studies, arc breakdowns of secondary arcs have mainly been considered as electrical breakdowns, ignoring the role of heat in the arc channel. Besides, the extinction-reignition theory of secondary arc, i.e., dielectric strength recovery theory, still lack the support of experimental data. In this study, based on the equivalent experiments performed in the laboratory, the influences of compensation degree of transmission lines, initial recovery voltage gradient of air gap, test current, wind speed, and wind direction on the breakdown characteristics of secondary arcs are studied and statistically analyzed. The laws of the transient recovery voltage (TRV) and of the rate of rise of recovery voltage (RRRV) also studied by considering the influencing factors mentioned above. The results of this study will provide a more complete experimental basis for the theory of extinction–reignition of secondary arcs and a deeper understanding of the transient characteristics of arc breakdown.**

***Index Terms*—secondary arc, extinction theory, arc breakdown, multiple reignition, single-phase-to-ground fault.**

I. Introduction

EHV/UHV transmission lines at 220 kV and above are an important part of the provincial transmission network in China. Experience with power grid operation has shown that more than 70% of short-circuit faults on high-voltage overhead lines above 110 kV with high-current grounding systems are single-phase-to-ground faults, with this figure reaching about 90% on overhead lines above 220 kV [1,2]. The reliability of the power supply and the stability of the parallel operation of the system can be greatly improved if a circuit breaker selectively disconnects the faulty phase, with the two healthy phases continuing to connect with the power system during the single-phase auto-reclosing (SPAR) period. After the fault is identified by the protection system, the faulty phase is tripped, and the short-circuit condition for the power system is eliminated. However, the arc plasma still exists at the faulty phase side, and that one is maintained by the healthy phases' currents [3,4]. However, after interruption of the faulty phase, if the secondary arc cannot be de-ionized and self-extinguished sufficiently within the setting time of SPAR of power system relay protection, the success rate of SPAR will be affected and the power supply will not be restored in time. Thus, the extinction–reignition characteristics of the secondary arc have a significant influence on the success rate of SPAR of power system relay protection and the transient stability of an EHV/UHV power system [1–13].

In recent years, results obtained using low-voltage experimental platforms to simulate multiple reignition of secondary arcs in EHV/UHV systems have provided a basis for studies of the laws of motion of cathode and anode arc roots and the arc column, studies of morphological characteristics (arc length, arc diameter, and centroid trajectory) [11,12,14–20], and studies of electrical characteristics (arc voltage–current waveform, arcing time, breakdown voltage, discharge energy, and volt–ampere characteristic) [2,8,12,14,21,22]. To determine the validity of low-voltage experimental simulations

This is a peer-reviewed, accepted author manuscript of the following research article:
Li, R., Liu, H., Lou, X., Song, P., Hou, W., Dai, S., Shi, Y., Jin, G., Siew, W. H., & Li, Q. (Accepted/In press). Study on the breakdown characteristics of multiple-reignition secondary arcs on EHV/UHV transmission lines. IEEE Transactions on Plasma Science, 1-13.
https://doi.org/10.1109/TPS.2023.3252799

in the laboratory, in [8,9], a statistical study of the influence of compensation degree of transmission lines, test current value, initial recovery voltage gradient of air gap, and wind speed on the 90% probability of secondary arc self-extinction was carried out, but there was no comprehensive analysis taking account of morphological characteristics. In [11], a low-voltage experimental simulation platform was established, the temporal evolution of the volt–ampere characteristic of a 10-A secondary arc during its multiple reignitions was investigated, and a combined analysis of arc discharge images, arc length variation, and breakdown voltage from the same set of experimental data was carried out. In [14], the volt–ampere characteristic and particle motion in an arc channel were investigated, and it was shown that changes in a number of electrical characteristics, including the volt–ampere characteristic, discharge energy, and arcing time, could be caused by short-cut events of arc column. Furthermore, the forced zero-crossing phenomenon of a secondary arc under the effect of wind was also quantitatively analyzed using energy balance theory [2,14,22], as another arc extinction-reignition theory for explaining the extinction-reignition phenomenon of secondary arc, in addition to the dielectric strength recovery theory [23,24].

Advances in arc image processing have greatly enriched research into the morphology of secondary arcs, and have made possible a comprehensive interpretation of electrical and morphological characteristics. There have also been advances in the development of algorithms for calculating the arcing time and statistical analyses of the factors that influence it. In [21], the factors exhibiting positive and negative correlations, respectively, with the arcing time of the secondary arc were determined through the use of an algorithm and a multivariate fitting procedure. In addition, a multivariate fitting was performed between the arcing time and the relevant factors, and a functional relationship was thereby obtained.

A secondary arc is essentially a plasma, exhibiting both electrical and thermal phenomena, and the latter have a strong effect on the electrical characteristics of the arc [25]. Thermal excitation and thermo-ionization involve the conversion of particle kinetic energy into potential energy (with the particles being excited or ionized) at a high temperature. At a high temperature, the large amount of photon energy radiated by thermal ionization will also produce photoionization, which helps to maintain and develop the secondary arc [26]. Therefore, thermal effects in the arc discharge process cannot be ignored, although previous studies have tended to ignore the role of heat in the breakdown of secondary arcs.

The remainder of this paper is organized as follows. In Section II, the low-voltage experimental simulation platform is introduced. In Section III, a division of the secondary arc discharge waveform into stages and a synthetic analysis of the discharge waveform and arc images are carried out, and the influences of the compensation degree, initial recovery voltage gradient and test current on the frequency distributions of electrical and thermal breakdown during arc reignitions are studied. In Section IV, using statistical data, a trend analysis of TRV and RRRV in arc reignitions is carried out, and the corresponding discrete data are also analyzed. Finally, in Section V, the influence of wind (the most significant of all external factors) on the extinction–reignition characteristics of the secondary arc is studied from the perspectives of its speed and direction.

The results of this study can provide experimental data and support for the study of extinction-reignition characteristics of secondary arc under the influence of different external conditions on EHV/UHV transmission lines. This paper also provides a more in-depth research direction for the transient characteristics of secondary arc.

II. EXPERIMENTAL SETUP

Based on the previous discussion on the low-voltage experimental platforms for simulating secondary arcs on EHV/UHV transmission lines, the experiments were conducted in the High Voltage Laboratory of the China Electric Power Research Institute [8,11]. The test circuit diagram is shown in Fig. 1.

The amplitude of the AC power supply was 11.6 kVrms, with 50-Hz power frequency, and its capacity was 3 MVA. By adjusting the electrode spacing of the insulator string, different initial recovery voltage gradients could be simulated. The insulator string was shorted by a 0.15-mm nichrome wire at both ends, and the inductance L_0 (36.88 mH) in the circuit was used to generate a 1-kA inductive short-circuit arc. When the inductance L_0 first formed a loop with the power supply, it melted the nichrome wire to create metallic vapor across the

insulator string, generating a short-circuit arc, from which it was easy to subsequently form a secondary arc. The inductance L_0 was then disconnected, and the parallel circuit of capacitor C and inductor L in the circuit was closed, and this was used to simulate a secondary arc on the undercompensated transmission line (I_L<I_C) and overcompensated transmission line (I_L>I_C). The inductor L was removed when a secondary arc on an uncompensated transmission line (I_L=0) was simulated [8].

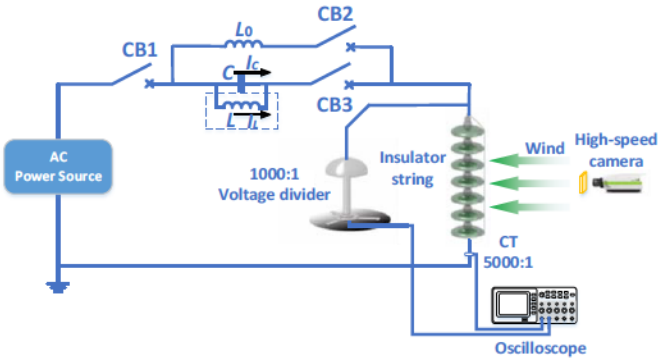

Fig. 1 Experimental scheme for the secondary arc, considering wind and compensation conditions.

In this study, secondary arcs with initial recovery voltage gradient conditions of 17.06 kV/m, 21.89 kV/m, and 30.53 kV/m (corresponding to electrode spacings of 68 cm, 53 cm, and 38 cm, respectively) as well as with test currents of 15 A, 30 A, and 45 A, by setting the values of inductance L and capacitor C, were separately investigated. The influences of wind speed and wind direction on secondary arc reignition were also examined. The tests were carried out at wind speeds of 0 m/s, 1.5 m/s, and 2.5 m/s, and the wind directions were from west to east (opposite to the Ampère force exerted on the secondary arc column) and from south to north (perpendicular to the Ampère force exerted on the secondary arc column). A diagram of the wind direction is shown in Fig. 2.

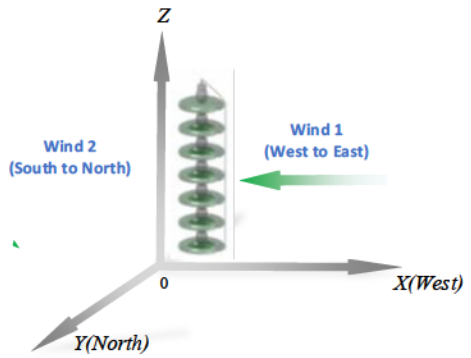

Fig. 2 wind direction in the tests.

A high-speed camera (Motion Pro Plus) with a frame rate of 500 frames/s (at 1280 × 1024 resolution) and a 6.5-s shoot time, equipped with a Nikon zoom lens (Nikon ED AF Nikkor 80–200 mm, 1:2.8 D), was used for tracking the movement of the secondary arc. The wind speed is measured by an anemometer (Tesco 405-V1).

III. Electrical and Thermal Breakdowns

A. Arc discharge waveforms and breakdown phenomenon of secondary arc

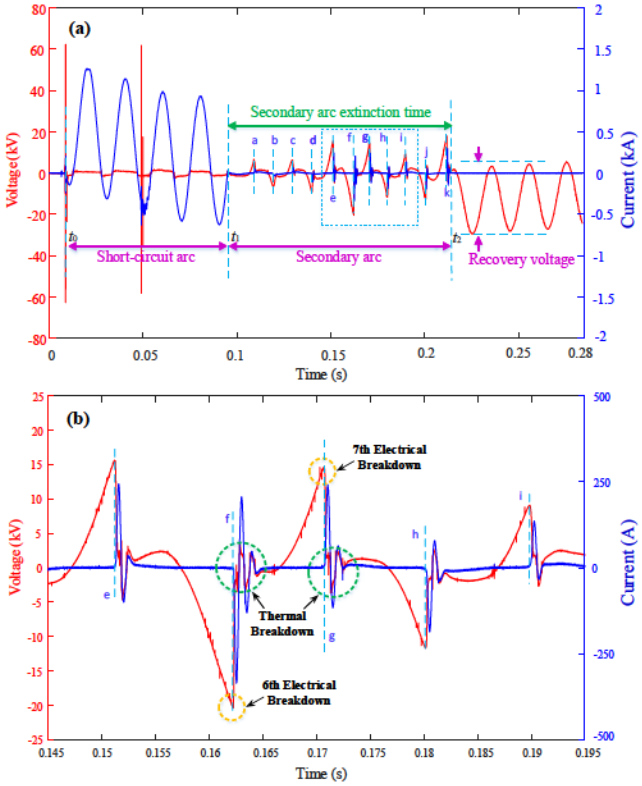

Fig. 3 (a) Multiple-reignition voltage and current waveforms of a secondary arc (15 A, no wind, uncompensated, and with initial recovery voltage gradient 30.53 kV/m). (b) Enlarged plot corresponding to the blue dotted rectangle in (a), showing successive thermal breakdowns.

Fig. 3(a) shows multiple-reignition voltage and current waveforms of a secondary arc. It can be seen from these waveforms that the secondary arc discharges with a total of eleven obvious electrical breakdowns, and it can be seen from Fig. 3(b) that the sixth and seventh of these are followed by several successive thermal breakdowns. The timescale of the

thermal breakdown process is about 1.5 ms. As shown in Fig. 3(a), a periodic sinusoidal bias voltage is finally formed between the arc gap after the completion of the last secondary arc discharge when an uncompensated transmission line is simulated. It should be noted that when a transmission line is compensated, the recovery voltage waveform after arc extinguishing will eventually have the phenomenon of beating frequency, and thus the waveform will be symmetric about the time axis.

Fig. 4 shows the electrical breakdowns of a 15-A secondary arc, corresponding to the electrical breakdowns indicated by the vertical blue dashed lines *a*, …, *k* in the secondary arc stage in Fig. 3(a). As can be seen, the metallic vapor outside the arc channel diffuses faster than the metallic vapor inside the arc channel with increasing time, the metallic vapor inside the arc channel is compacted owing to self-magnetic compression. The arc column moves toward the upper-right direction, mainly under the effects of electromagnetic force and thermal buoyancy [14,20,22], and a short-cut event occurs at the moments *d*, *e* and *f* in the arc channel with rises in electrical breakdown voltage, as shown in Fig.3(a). Normally, the arc channel reaches its maximum arc length at the final electrical breakdown *k* according to the maximum critical length criterion of secondary arc [11,20,22].

Whether the arc reignites or not after current zero-crossing is determined by the recovery voltage applied on the arc channel [8,9,23,24]. Normally, there are two opposing processes occurring repeatedly during arc multiple reignitions. One, which leads to an increase in arc channel conductivity, is ionization of neutral particles due to the action of the electric field and to thermal ionization after secondary arc ignition. The other, which leads to an increase in arc resistance, is due to wind, convective cooling, and recombination and diffusion of particles causing an increased rate of recovery of dielectric strength in the arc gap. In addition, the voltage necessary for breakdown increases because the secondary arc is drawn out by wind, thermal buoyancy, and the electromagnetic force, and resulting an increasement of contact area between arc column and ambient air, which enhances the de-ionization process.

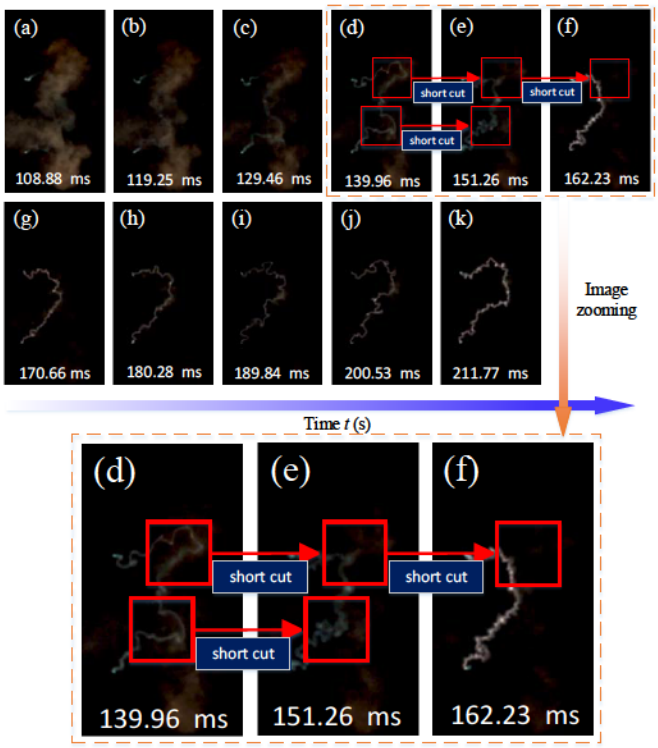

Fig.4 Electrical breakdowns of a 15-A secondary arc, corresponding to the vertical blue dashed lines in the secondary arc stage in Fig. 3(a).

B. Factors influencing thermal breakdown and electrical breakdown in the secondary arc discharge stage

1) Compensation degree

In this study, electrical and thermal breakdown of 15-A uncompensated and undercompensated secondary arcs at an electrode spacing of 38 cm (an initial voltage gradient of 30.5 kV/cm) are shown in Figs. 5(a) and 5(b). In a total of ten samples of overcompensated tests, electrical breakdown and thermal breakdown occurred in only one test sample (not shown in Fig. 5). With increasing compensation degree, as shown in Figs. 5(a) and 5(b), the number of secondary arc discharge samples and the number of reignition times in each test sample decreased significantly.

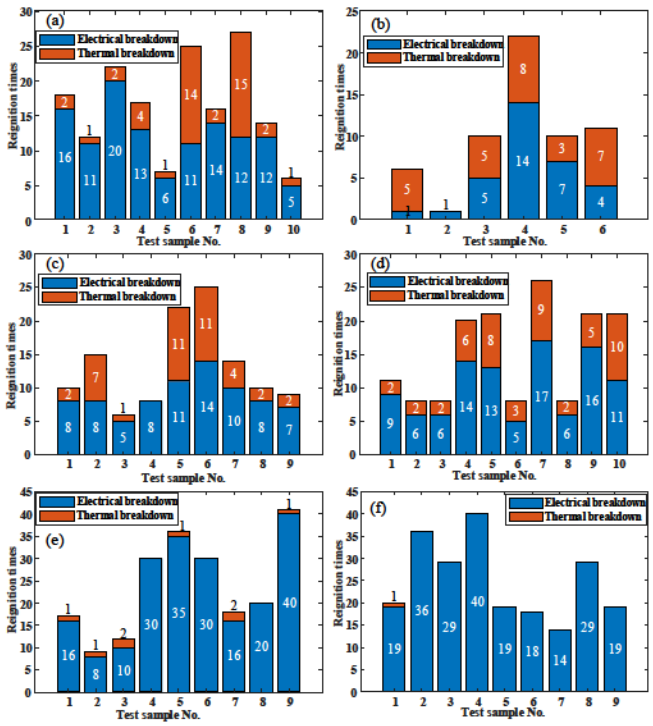

Fig. 5 Statistical results on electrical and thermal breakdown during multiple reignition of secondary arcs under windless conditions: (a) 15-A uncompensated and (b) 15-A undercompensated secondary arcs with 38-cm electrode spacing; (c) and (d) 15-A uncompensated secondary arcs with 53-cm and 68-cm electrode spacing, respectively; (e) 30-A and (f) 45-A uncompensated secondary arcs with 53-cm electrode spacing. The number of tests generating secondary arc and the number of total experiments of each different test conditions can be seen in TABLE I, TABLE II, and TABLE III (the column of *probability of arcing*).

2) Initial recovery voltage gradient

The statistical results for the breakdown of 15-A secondary arcs at electrode spacings of 38 cm, 53 cm, and 68 cm (corresponding to initial recovery voltage gradients of 30.53 kV/m, 21.89 kV/m, and 17.06 kV/m) are shown in Figs. 5(a), 5(c), and 5(d), respectively. Within the range of electrode spacings tested, it can be seen that the spacing or the initial recovery voltage gradient has no significant effect on the number of samples in which discharge occurred, or on the number of reignitions in a single discharge sample.

3) Test current of secondary arc

Figs. 5(c), 5(e), and 5(f) show statistical results for electrical and thermal breakdown of 15-A, 30-A, and 45-A secondary arcs, respectively, all with an electrode spacing of 53 cm. Increasing the test current of the secondary arc will increase the discharge energy, thereby increasing the number of samples in which discharge occurred and the number of electrical breakdowns and reducing the number of thermal breakdowns. For 30-A and 45-A secondary arc test currents, the dielectric strength across the arc gap does not recover sufficiently, resulting in more electrical breakdowns than the experiments under 15-A test current conditions during reignitions. In EHV and UHV systems, when the secondary arc current is lower than 30 A, the arc discharge normally tends to self-extinguish [8].

IV. TRV AND RRRV IN SECONDARY ARC REIGNITIONS

Based on the dielectric strength recovery theory, gap breakdown and arc reignition will occur in the arc channel when the recovery rate of the dielectric strength is lower than the RRRV [23,24]. The breakdown voltage of the arc gap is equal to the TRV at the moment of gap breakdown. Therefore, the recovery rate of the gaseous medium can be measured by the RRRV of the arc gap at the moment of gap breakdown, i.e., when the RRRV of the arc gap just exceeds the recovery rate of the gaseous medium. The RRRV is calculated as follows:

$$RRRV = \frac{TRV}{t_q} \tag{1}$$

here, t_q is the time difference between the moment at which the TRV zero value starts rising and the moment at which the TRV reaches its peak value, and is basically equal to half of the power cycle (10 ms) during the multiple-reignition process, and hence the trend of variation of the RRRV is basically consistent with that of the TRV.

Figs. 6, 7, and 8 show the influences of compensation degree, initial recovery voltage gradient, and test current of the secondary arc, respectively, on the TRV and the RRRV during the multiple-reignition process. The test sample number indicated by arrows in Figs. 6–8 corresponds to those in Fig. 5.

1) Compensation degree

High-voltage shunt reactors are normally installed on EHV/UHV transmission lines, not only reduce the line natural shunt capacitive effect that will result in a sustained overvoltage at light-loading operation conditions, but also play a role as the most important source that maintains the secondary arc. The voltage, current, and other electrical characteristics of the secondary arc will all depend on the compensation degrees

of the transmission lines with these shunt reactors. Because of the variability in arc discharge, it is necessary to perform statistical analyses on data from test samples of secondary arcs [19].

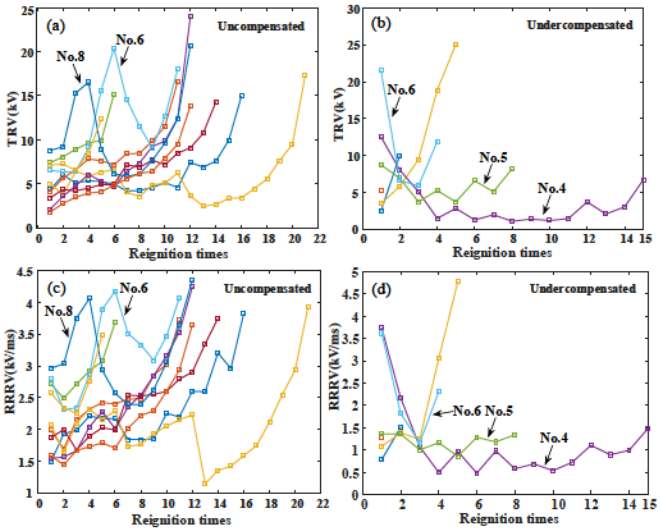

Fig. 6 Curves of variation of TRV and RRRV during multiple reignition of a 15-A secondary arc with 38-cm electrode spacing (30.53-kV/m recovery voltage gradient), under conditions of no compensation [(a) and (c)] and undercompensation [(b) and (d)].

In Figs. 6(a) and 6(c), the recovery voltages of sample data Nos. 6 and 8 drop sharply in part of each curve. The voltage and the current waveforms and the discharge images of sample data No.6, corresponds to the multiple reignitions shown in Figs. 3(a) and (b) and Fig. 4. Combined with the corresponding voltage and current waveforms, the thermal breakdowns in test sample occurred many times, with two or three thermal breakdowns occurred immediately after each electrical breakdown during the reignition process, corresponding to the decline stage in Fig. 6(a).

From the voltage and current waveforms of sample data No.6 [Fig. 3(b)], it can be seen that the TRV value reached 20.35 kV at the sixth electrical breakdown, which was followed by three thermal breakdowns. The number of conductive particles generated in the arc channel is more than in the previous two adjacent electrical breakdowns, owing to the thermal breakdowns, and the existence of the multiple thermal breakdowns makes the zero-crossing time shorter than the normal zero-crossing time. Consequently, the recovery time of the dielectric strength will also be shorter, and therefore the breakdown voltage required for the next electrical breakdown will be lower. Thus, on the one hand, the thermal breakdown process can shorten the recovery time of the dielectric, and on the other hand, it can keep the arc channel at a high ionization degree during the adjacent electrical breakdown. Therefore, when multiple thermal breakdowns occur between two adjacent electrical breakdowns, the TRV and RRRV at the latter electrical breakdown tend to decrease. It can also be seen from Fig. 5(a) that thermal breakdown accounted for the largest proportion in sample data Nos. 6 and 8, occurring 14 and 15 times, respectively, by comparing with other tests in the same test group.

In Figs. 6(b) and 6(d), sample data Nos. 4, 5, and 6 for the 15-A undercompensated secondary arc all show a decreasing trend in the TRV during the initial secondary arc stage. The discharge images at this time show that repetitive short-cut events are present during the initial stage of the secondary arc. After the short-circuit arc, the metallic vapor outside the arc channel does not diffuse significantly during the initial stage of the secondary arc. If there is no significant isolation of conductive particles inside and outside the arc channel, a short-cut event may occur during arc reignition, which will extending the process of arc self-elongation. With the increase in reignition times, the arc as a whole becomes elongated, mainly through the action of wind, the electromagnetic force, and thermal buoyancy, and the TRV at the moment of gap breakdown tends to rise, finally reaching a maximum at the moment of arc extinction. Likewise, the recovery rate of dielectric strength follows the same trend during multiple reignitions.

Generally, the probability distribution of the secondary arc discharge time, under the same experimental conditions, follows a normal distribution. However, because the standard deviation σ of the arcing time of the secondary arc is unknown, it must be replaced by the sample standard deviation s, and so the distribution becomes a t-distribution rather than a normal distribution. Using the t-distribution, the arcing time of the secondary arc with 90% confidence coefficient can be calculated as follows:

$$\mu = \bar{x} \pm \frac{t_{\alpha,f} \cdot s}{\sqrt{n}} \tag{2}$$

$$f = n - 1 \tag{3}$$

$$\alpha = 1 - p \tag{4}$$

where μ and $\bar{x}$ are the expected value and mean value of the secondary arc arcing time, f is the degree of freedom, n is the number of test samples, α is the significance level, and p is the confidence coefficient (here is 90%), $t_{\alpha,f}$ is the value looked up in the t-table when α and f are known, and s is the sample standard deviation of the secondary arc arcing time. The 90% probability arcing time ranges of secondary arcs with different compensation degrees of transmission lines are shown in Table I.

TABLE I

STATISTICS OF EXPERIMENTAL RESULTS ON MULTIPLE-REIGNITION CHARACTERISTICS OF SECONDARY ARCS UNDER DIFFERENT COMPENSATION CONDITIONS

Compensation condition	Mean value of arcing time (s)	90% probability arcing time range (s)	Mean value of zero-crossing time (s)	Mean value of maximum recovery voltage after extinction (kV)	Probability of arcing
Uncompensated	0.1276	0.1102–0.1528	0.0025	28.655	10/10
Undercompensated	0.07947	0.0338–0.1251	0.0057	27.576	6/10
Overcompensated	0.0444	/	0.0299	24.837	1/10

The test current value of the secondary arc is 15 A, with 30.53-kV/m initial recovery voltage gradient.

On the basis of the statistical results in Table I and Fig. 6, it is found that the arcing time, reignition times, and maximum recovery voltage after arc extinction exhibit an obvious downward trend with increasing compensation degree. The zero-crossing time rises with increasing compensation degree. Generally, the larger the zero-crossing time, the fewer are the reignitions. The statistical results of this study show that the probability of arc reignition decreases with increasing compensation degree of transmission lines. A high compensation degree can effectively reduce the possibility of arc reignitions by increasing the zero-crossing time and thus shortening the arcing time of the secondary arc.

2) Initial recovery voltage gradient

With a constant applied voltage applied between the electrodes, variations in the electrode spacing will affect the electric field intensity in the arc channel. With increasing electrode spacing, the electrical breakdown voltage also rises, and so does the maximum arc current value, i.e., the breakdown current. In fact, the value of the maximum arc current can be used to represent the intensity of the discharge.

Overall, the TRV and RRRV curves show an upward trend. Sample data Nos. 5 and 6 in Fig. 7(a) and Nos. 5–7 and 9–10 in Fig. 7(b) all show that the TRV drops significantly at electrical breakdowns. The sample data groups with large drops in the TRV and RRRV curves are the experimental groups with more thermal breakdowns, on the basis of the statistical results shown in Figs. 5(c), 5(d), and 7. From the corresponding voltage and current waveforms during the late stage of reignition, it is found that the sharp drops in the TRV at the electrical breakdowns occur after several consecutive thermal breakdowns. The ionization degree across the arc channel is still very high at this time, and, in addition, the thermal breakdown process shortens the recovery time of dielectric strength. Moreover, the arc column during the later stage of reignition is drawn out such that the arc channel overlaps within the diffused metallic vapor, driven by thermal buoyancy and the electromagnetic force. In terms of arc morphology as described by the maximum critical length of the secondary arc, arc column short-cut events can also prolong the discharge time [14]. Considering Figs. 6 and 7, comparisons of the number of short-cut events with reignition times from the same sample data show that if the short-cut events occur in the secondary arc stage, they are very likely to prolong the duration of this stage. The reignition times (proportional to the arcing time) of sample data Nos. 5 and 6 in Fig. 7(a) and Nos. 5–7, 9, and 10 in Fig. 7(b) are all higher than those of other test samples under the same experimental conditions.

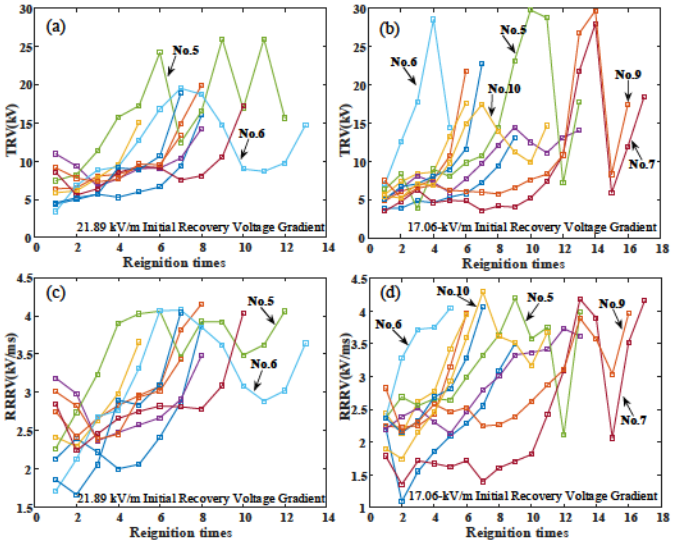

Fig. 7 Curves of variation of TRV and RRRV during multiple reignition of a 15-A secondary arc with [(a) and (c)] 53-cm electrode spacing (21.89-kV/m recovery voltage gradient) and [(b) and (d)] 68-cm electrode spacing (17.06-kV/m recovery voltage gradient), under conditions of no compensation.

TABLE II

STATISTICS OF EXPERIMENT RESULTS ON MULTIPLE-REIGNITION CHARACTERISTICS OF SECONDARY ARCS FOR DIFFERENT INITIAL RECOVERY VOLTAGE GRADIENTS

Initial recovery voltage gradient (kV/m)	Mean value of arcing time (s)	90% probability arcing time range (s)	Mean value of zero-crossing time (s)	Mean value of maximum recovery voltage after extinction (kV)	Probability of arcing
30.53	0.1276	0.1102–0.1528	0.0025	28.655	10/10
21.89	0.0969	0.08223–0.1116	0.0038	28.442	10/10
17.06	0.1138	0.08940–0.1382	0.0034	28.332	10/10

The test current of the secondary arc is 15 A, under a condition of no compensation.

From the statistical results on electrical characteristics in Table II, there does not appear to be any obvious trend of variation of the average discharge time and zero-crossing time of the secondary arc, although the maximum recovery voltage after extinction decreases slightly with increasing initial recovery voltage gradient.

3) Test current of secondary arc

Normally, for a constant test voltage, the electrostatic induction component of the secondary arc, derives from the equivalent capacitance C between the faulty phase and the healthy phase of the transmission lines, is proportional to the length of the line. Thus, the longer the line (or the higher the capacitive coupling), the higher is the secondary arc current.

The curves of variation of the TRV and RRRV during multiple reignitions of 30-A and 45-A secondary arcs are shown in Fig. 8. The TRV and the RRRV show increasing trends as the arc reignitions proceed. It should be noted that the decreases in the TRV and RRRV in test sample No. 1, marked by arrows in Figs. 8(b) and 8(d), are due to the thermal breakdown after the 18th electrical breakdown. Thermal breakdown shortens the recovery time of dielectric strength across the air gap, while, on the other hand, maintaining the arc channel at a high ionization degree for a period of time and thus reducing the breakdown voltage of the next arc discharge.

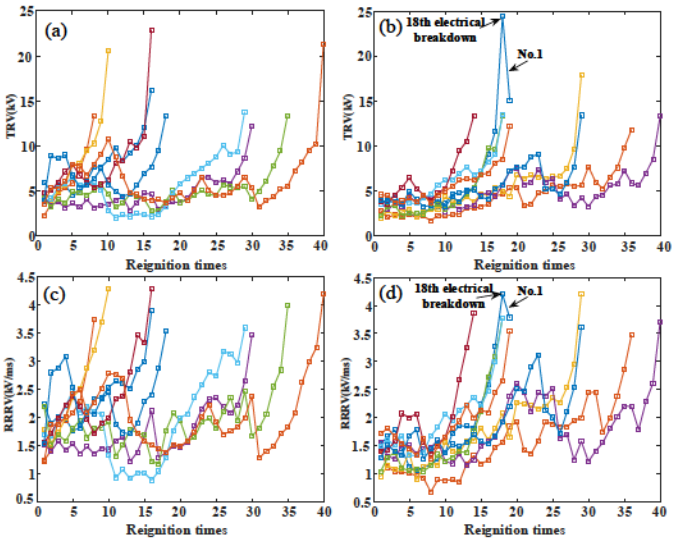

Fig. 8 Curves of variation of TRV and RRRV during multiple reignition of [(a) and (c)] 30-A and [(b) and (d)] 45-A secondary arcs, with 53-cm electrode spacing (21.89-kV/m recovery voltage gradient), under conditions of no compensation.

The reignition times in a single test sample increase significantly with increasing test current, but the maximum values of the TRV and the RRRV remain almost unchanged, as can be seen in Figs. 7(a), 7(c), and 8. As shown in Table III, as the test current increases, the reignition times of the secondary arc increase significantly, whereas the zero-crossing time decreases, and the maximum recovery voltage after arc extinction also decreases to a certain extent. The shorter the zero-crossing time, the slower is the recovery process of the dielectric strength, and the more frequent are the arc reignitions.

Multi-batch experiments and operation experiences in China show that when uncompensated secondary arc current is about 10-12 A (the RMS value of its fundamental wave), the secondary arc will quickly self-extinguished within 0.2 s [8], which is consistent with the experiment result of 15-A secondary arc in the order of magnitude, shown in Table III.

TABLE III

STATISTICS OF EXPERIMENTAL RESULTS ON MULTIPLE-REIGNITION CHARACTERISTICS OF SECONDARY ARCS FOR DIFFERENT TEST CURRENTS

Test current (A)	Mean value of arcing time (s)	90% probability arcing time range (s)	Mean value of zero-crossing time (s)	Mean value of maximum recovery voltage after extinction (kV)	Probability of arcing
15	0.0969	0.08223–0.1116	0.0038	28.442	10/10
30	0.2344	0.1724–0.2964	0.0014	27.680	9/9
45	0.2559	0.2059–0.3059	0.00079	26.029	11/11

The initial recovery voltage gradient of the secondary arc is 21.89 kV/m under a condition of no compensation. The secondary arc in two test samples failed to extinguish in all 11 test samples when the test current was 45 A.

V. WIND FACTORS AFFECTING SECONDARY ARC

According to multifield coupled dynamic modeling of secondary arcs, the secondary arc column is affected mainly by the electromagnetic force, wind force, and air resistance in the horizontal direction, and by thermal buoyancy in the vertical direction [20]. Wind can accelerate the de-ionization and thermal convection processes of the secondary arc, and the arc column will be lengthened, weakening the thermal ionization degree in the arc channel. Recombination between particles is strengthened and the difficulty of reignition is evidently increased. In this study, electrical breakdown of the secondary arc was investigated at different wind directions and wind speeds, and statistical plots of the RRRV are shown in Fig. 9. It can be seen that with increasing reignition times, the RRRV shows an overall increasing trend, although there are local decreases in the RRRV due to thermal breakdown between two adjacent electrical breakdowns.

The wind direction diagram is shown in Fig. 2. A comparison between Figs. 9(a) and 9(c) on the one hand and Fig. 9(b) and (d) on the other hand shows that when the wind direction is from west to east (i.e., opposite to the Ampère force exerted on the secondary arc column), the number of arc discharge test samples is significantly more than when the wind direction is from south to north (i.e., perpendicular to the Ampère force exerted on the secondary arc column).

As shown in Table IV, with increasing wind speed, the average value of the arcing time tends to decrease, whereas the zero-crossing time tends to increase, and the maximum recovery voltage after arc extinction decreases to a certain extent. A longer zero-crossing time indicates that the secondary arc needs to achieve a higher RRRV for arc breakdown to occur, and so the probability of arc reignition becomes smaller. As can be seen from Fig. 9(d), a high RRRV occurred in test sample No. 6, because no arc breakdown occurred at the previous voltage peak before the seventh electrical breakdown. When the voltage rises in reverse with periodic change, the recovery voltage across the air gap rises to the breakdown voltage, and the seventh electrical breakdown occurs.

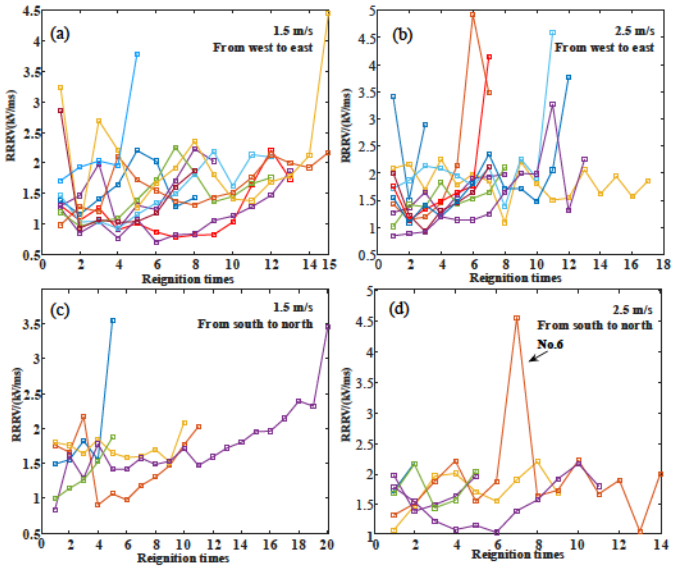

Fig. 9 Curves of variation of RRRV during multiple reignitions of a 30-A secondary arc for 68-cm electrode spacing (17.06-kV/m recovery voltage gradient), under a condition of undercompensation: (a) and (c) 1.5-m/s wind speed with wind direction from west to east and from south to north, respectively; (b) and (d) 2.5-m/s wind speed with wind direction from west to east and from south to north, respectively.

TABLE IV

STATISTICS OF EXPERIMENTAL RESULTS ON MULTIPLE-REIGNITION CHARACTERISTICS OF SECONDARY ARCS UNDER WIND CONDITIONS

Wind speed (m/s)	Wind directions	Mean value of arcing time (s)	90% probability arcing time range (s)	Mean value of zero-crossing time (s)	Mean value of maximum recovery voltage after extinction (kV)	Probability of arcing
1.5	From west to east	0.12296	0.1040~0.1419	0.0028	28.4601	10/10
2.5	From west to east	0.11115	0.08730~0.1350	0.0040	28.2452	10/10
1.5	From south to north	0.11154	0.07363~0.14944	0.0020	29.0132	5/10
2.5	From south to north	0.08778	0.05455~0.1210	0.0034	28.2388	6/10

The test current of the secondary arc is 30A, under a condition of undercompensation with 17.06-kV/m initial recovery voltage gradient.

Statistical results for electrical and thermal breakdown of a secondary arc for different wind speeds and wind directions are shown in Fig. 10. Comparisons between Figs. 10(a) and 10(b), and between Figs. 10(c) and 10(d), show that the number of samples in which discharge occurred does not change significantly with increasing wind speed.

From Fig. 10 and Table IV, it can be seen that when the wind direction is from west to east (i.e., opposite to the Ampère force exerted on the secondary arc column), the action of the wind hinders self-elongation of the arc, resulting in greater numbers of electrical and thermal breakdowns at a given wind speed.

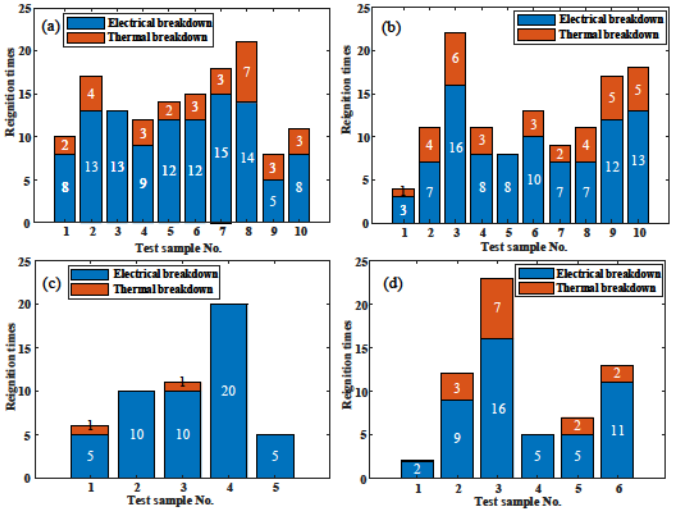

Fig. 10 Statistical results on electrical and thermal breakdown during multiple reignition of 30-A undercompensated secondary arc with 68-cm electrode spacing (17.06-kV/m recovery voltage gradient) under windy conditions: (a) and (c) 1.5-m/s wind speed with wind direction from west to east and from south to north, respectively; (b) and (d) 2.5-m/s wind speed with wind direction from west to east and from south to north, respectively.

By contrast, when the wind direction is from south to north (perpendicular to the Ampère force exerted on the secondary arc column), the wind accelerates the self-elongation, and the numbers of electrical and thermal breakdowns decrease sharply, and there is also some decrease in the arcing time, although the zero-crossing time and maximum recovery voltage gradient after arc extinction do not change significantly.

VI. Conclusions

A low-voltage experimental platform for simulation of secondary arcs in the laboratory was established. The probabilities and numbers of electrical and thermal breakdowns as well as the trends of variation of the TRV and RRRV during secondary arc reignitions were studied in detail. The following conclusions were drawn from the results of these investigations:

1) During the multiple-reignition process, the TRV and RRRV show overall increasing trends, although they exhibit temporary decreases due to thermal breakdowns. On the one hand, thermal breakdown shortens the recovery time of dielectric strength in the arc channel, while, on the other hand, maintaining the arc channel at a high ionization degree for a period of time and thus reducing the breakdown voltage of the next electrical breakdown.
2) When the compensation degree of transmission lines is increased, the arcing time, reignition times, and maximum recovery voltage after arc extinction all show distinct downward trends, meaning that the probability of arc reignition is lower. The zero-crossing time is negatively correlated with the probability of arc reignition, and it increases with increase of compensation degree of transmission lines. A short-cut event may occur during arc reignition, which will extending the process of arc self-elongation.
3) Within the wind speed range in this study, the probability of arc reignition does not decrease with increasing wind speed, but the arcing time is reduced. At a given wind speed, when the wind force is opposite to the Ampère force on the arc column, which reduces the self-elongation of the arc and

increases the arcing time. When the wind force is perpendicular to the Ampère force on the arc column, enhancing the elongation of the arc and making it easier to extinguish.

REFERENCES

[1] H. Cong, S. Wang, D. Han, H. Pan, and Q. Li, "Study on the influence of injected lightning current on the space-time evolution of secondary arc," *IEEE Trans. Ind. Appl.*, vol. 57, no. 5, pp. 4537–4547, Sept.–Oct. 2021.

[2] H. Cong, Q. Li, J. Xing, J. Li, and Q. Chen, "Computation Method of Arcing Time of the Secondary Arcs Based on Energy Balance," *Proc. CSEE*, vol. 35, no. 13, pp. 3450–3458, Jul. 2015.

[3] A. T. Johns and A. M. Al-Rawi. "Developments in the simulation of long-distance single-pole-switched EHV systems." *IEE Proc.*, vol. 131, no. 2, pp. 67–77, Mar. 1984.

[4] J. Klucznik, Z. Lubosny, K. Dobrzynski, and S. Czapp, "Secondary arc modelling for single pole reclosing analyses," in *2015 IEEE Power & Energy Society General Meeting*, 2015, pp. 1–5, doi: 10.1109/PESGM.2015.7286186.

[5] J. Han, C. Lee, and C. Kim, "Adaptive single-pole auto-reclosing scheme based on secondary arc voltage harmonic signatures," *Energies*, vol. 14, no. 5, Feb. 2021, https://doi: 10.3390/en14051311.

[6] O. Dias, F. Magrin, and M. C. Tavares, "Comparison of secondary arcs for reclosing applications," *IEEE Trans. Dielectr. Electr. Insul.*, vol. 24, no. 3, pp. 1592–1599, Jun. 2017.

[7] T. Tsuboi, J. Takami, S. Okabe, K. Aoki, and Y. Yamagata, "Study on a field data of secondary arc extinction time for large-sized transmission lines," *IEEE Trans. Dielectr. Electr. Insul.*, vol. 20, no. 6, pp. 2277–2286, Dec. 2013.

[8] Y. He, G. Song, R. Cao, Y. Yuan, J. Lin, L. Ban, W. Li, K. Yang, and B. Han, "Test research of secondary arc in 1 000 kV UHV double-circuit transmission lines" *Proc. CSEE*, vol. 31, no. 16, pp. 138–143, Jun. 2011.

[9] Y. He, G. Song, and R. Cao, "The equivalence research for secondary arc simulation test of UHV with double circuit transmission lines", *Power Syst. Technol.* vol. 32, no. 22, pp. 4–7, Nov. 2008.

[10] Q. Sun, Z. Xiao, H. Liu, Q. Li, and F. Wang, "A study on the transient of secondary arc current of UHV transmission lines," *IEEE Access*, vol. 6, pp. 38616–38626, Jul. 2018.

[11] H. Liu, R. Li, D. He, J. Wei, and Q. Li, "Experimental study of multiple-reignition features of secondary arcs on EHV/UHV transmission lines," *IEEE Trans. Ind. Electron.*, vol. 66, no. 4, pp. 3247–3255, Apr. 2019.

[12] H. Cong, D. Han, S. Wang, L. Qiao, and Q. Li, "Experimental study on the extinction characteristics of secondary arc under different secondary arc currents near outdoor insulator," *IEEE Trans. Dielectr. Electr. Insul.*, vol. 29, no. 1, pp. 103–110, Feb. 2022.

[13] H. Liu *et al.*, "Influence of hybrid reactive power compensation on the secondary arc of ultra-high-voltage transmission lines (May 2018)," *IEEE Access*, vol. 6, pp. 38115–38123, 2018.

[14] Q. Sun *et al.*, "Investigation on volt–ampere characteristic of secondary arc burning in atmospheric air," *Phys. Plasmas*, vol. 25, no. 9, p. 093513, Sep. 2018.

[15] Q. Sun, F. Liang, F. Wang, H. Cong, Q. Li, and J. Yan, "Investigation on the geometrical characteristics of secondary arc by image edge detection," *IEEE Trans. Plasma Sci.*, vol. 46, no. 6, pp. 2016–2025, Jun. 2018.

[16] T. Xia, H. Liu, Z. Xue, L. Ji, H. Cong, and Q. Li, "The movement characteristics and the plasma state of secondary arc," in *2018 China International Conference on Electricity Distribution (CICED)*, pp. 1615–1619, 2018.

[17] T. Xia, H. Liu, R. Li, Q. Sun, Q. Li, and H. Cong, "Edge detection and morphological characteristics analysis of secondary arc simulation experiment image," *Proc. CSEE*, vol. 39, no.3, pp. 923–932, Feb. 2019.

[18] R. Li, H. Liu, J. Lou, Q. Sun, X. Ma, and Q. Li, "Investigation on electrical characteristics and arc column morphology of secondary arc on UHV transmission lines," *High Voltage Eng.*, vol. 44, no. 4, pp. 1359–1366, Apr. 2018.

[19] Q. Li, J. Xing, H. Cong, Q. Chen, J. Li, and Q. Li, "Arc simulation model with consideration of the initial position randomness of the secondary arc," *High Voltage Eng.*, vol. 41, no. 6, pp. 1898–1906, Jun. 2015.

[20] J. Xing, Q. Li, H. Cong, Q. Chen, J. Li, and Q. Li, "Research on multi-field coupled dynamic modeling of secondary arcs with half-wavelength transmission lines," *Proc. CSEE*, vol. 35, no. 9, pp. 2351–2359, May 2015.

[21] H. Liu, Z. Zhang, T. Xia, J. Yang, Q. Li, D. He, and Y. Wang, "Investigation on the influencing factors of arcing time for secondary arcs," *IEEE Trans. Ind. Electron.*, doi: 10.1109/TIE.2021.3127019.

[22] H. Cong, Q. Li, J. Xing, J. Li, and Q. Chen, "Critical length criterion and the arc chain model for calculating the arcing time of the secondary arc related to AC transmission lines," *Plasma Sci. Technol.*, vol. 17, no. 6, pp. 475–480, Jun. 2015.

[23] J. Slepian, "Extinction of a long A-C. arc," *Trans. Am. Inst. Electr. Eng.*, vol. 49, no. 2, pp. 421–430, Apr. 1930, doi: 10.1109/T-AIEE.1930.5055517.

[24] J. Slepian, "Extinction of an A-C. arc," *Trans. Am. Inst. Electr. Eng.*, vol. 47, no. 4, pp. 1398–1407, Oct. 1928, doi: 10.1109/T-AIEE.1928.5055155.

[25] X. Yan, W. Chen, Z. He, C. Wang, J. Wu, and J. Wang, "Temperature measurement of air arc in long gap by spectrum diagnosis," *Proc. CSEE*, vol. 31, no. 19, pp. 146–152, Jul. 2011.

[26] D. Xiao, "Dielectric strength of atmosphere air," in *Gas Discharge and Gas Insulation*. Shanghai, China: Shanghai Jiao Tong University Press/Springer, ch. 4, 2017.

Runchang Li, was born in Hefei, China. He received the M.S. degree in high-voltage and insulation engineering with Shandong University, Jinan, China, in 2018. He is currently working at State Grid Hangzhou Power Supply Company, Hangzhou, China. His current research interests include arc discharge theory and its applications, power system relay protection, electromagnetic transient analysis as well as its inhibitions.

Hongshun Liu (M'17), was born in Qingdao, Shandong, China. He received the B.Sc. and Ph.D. degrees in electrical engineering from Shandong University, Jinan, China, in 2004 and 2010, respectively. He is currently an Associate Professor of electrical engineering with Shandong University. His research interests include the modeling and simulation for power system electromagnetic transient processes, overvoltage and insulation coordination, and arc discharge theory and its application (secondary arc and switching arc in UHV power system).

Xiaoxuan Lou, received the B.S. degrees in electrical engineering from Huazhong University of Science and Technology, Hubei, China, in 2012, and the M.S. degrees from both Chongqing University and University of Wisconsin-milwaukee. He is currently working at State Grid Hangzhou Power Supply Company, Hangzhou, China. His current research interests include power system relay protection.

Ping Song, was born in Hangzhou, China, received the B.Sc. degree in electrical engineering from the Hangzhou Dianzi University. He is currently working at State Grid Hangzhou Power Supply Company, Hangzhou, China. His current research interests include power system relay protection and substation automation technology.

WeiHong Hou, was born in Jiang Xi, China, received the M.S. degree in power system and its automation with Shanghai Jiao Tong University, Shanghai, China, in 2010. He is currently working at State Grid Hangzhou Power Supply Company, Hangzhou, China. His current research interests include power system relay protection and smart substation technology.

Shiqiang Dai, was born in Haian, China, received the M.S. degree in electrical engineering from Tsinghua University, Beijing, China, in 2011. His current research interests include power system relay protection, construction of new power system and impact of new energy resources.

Yuchao Shi, was brorn in Ningbo, China, received Ph.D. degree in electrical engineering from Tsinghua University, Beijing, China, in 2013. His current research interests include power electronics and power drives and China's new power system.

Gongyu Jin, was born in Huzhou, China. He received the M.S. degree in power system and its automation with Zhejiang University, Hangzhou, China. He is currently working at State Grid Hangzhou Power Supply Company, Hangzhou, China. His current research interests include power system relay protection.

Wah Hoon Siew (M'95), received the B.Sc (Hons.) degree in electronic and electrical engineering, the Ph.D. degree in electrical engineering, and the

Master of Business Administration from the University of Strathclyde, Glasgow, U.K., in 1978, 1982, and 1985, respectively. Currently, he is a professor in the Department of Electronic and Electrical Engineering at the University of Strathclyde, where he has been since 1989. Prof. Siew is a member of the IEE, a chartered electrical engineer and chartered engineer in the U.K., and serves several international working groups and panels including CIGRE and the IET.

Qingmin Li (M'07), received the B.Sc., M.Sc., and Ph.D. degrees in electrical engineering from Tsinghua University, Beijing, China, in 1991, 1994, and 1999, respectively.

He is currently a professor in electrical engineering with North China Electric Power University, China. He was with Tsinghua University as a Lecturer in 1996, and came to U.K. in 2000 as a Postdoctoral Research Fellow working with Liverpool University and later with Strathclyde University. He was with Shandong University in 2003 and worked there as a professor in electrical engineering till 2011. He was with the Arizona State University, USA, as a Visiting Professor from February to August 2010. His research interests include high-voltage engineering, applied electromagnetics, condition monitoring and fault diagnostics, high-voltage power electronics, etc.

Prof. Li is a Member of IET.